Modelling of a Free-Piston Generator Based on Spark-Ignition Engine, Linear Electric Machine and Active Rectifier

Alberto Dolara
Department of Energy
Politecnico di Milano
Milan, Italy
alberto.dolara@polimi.it

Giovanni Gaetano Gianetti
Department of Energy
Politecnico di Milano
Milan, Italy
giovannigaetano.gianetti@polimi.it

Sonia Leva
Department of Energy
Politecnico di Milano
Milan, Italy
sonia.leva@polimi.it

Tommaso Lucchini
Department of Energy
Politecnico di Milano
Milan, Italy
tommaso.lucchini@polimi.it

Andrea Facheris
Department of Energy
Politecnico di Milano
Milan, Italy
andrea1.facheris@mail.polimi.it

Francesco Fasana
Department of Energy
Politecnico di Milano
Milan, Italy
francesco.fasana@mail.polimi.it

***Abstract*—The Free-Piston Linear Generator (FPLG) technology is meant to serve as a link between the period of fossil fuels and the next green power generation. It consists of a Free-Piston Internal Combustion Engine (ICE) mechanically coupled with a Linear Electric Machine (LEM). No constraints on the piston movement and the inherently variable Compression Ratio (CR) result in a low vibrations, low friction, low maintenance costs, multifuel and high efficiency ICE, with a significant reduction of fuel consumption and greenhouse-gas emissions. In this paper the modelling of this new electricity generation system is investigated. The models of a gasoline single-piston Spark Ignition (SI) Free-Piston ICE and of the electric conversion system based on a three-phase LEM and a Space Vector Pulse Width Modulation (SVPWM) controlled active rectifier are developed in the CFD open-source OpenFOAM and Matlab Simulink environments, respectively.**

***Index Terms*—free piston; rectifier, thermodinamic simulation, Space Vector Pulse Width Modulation**

I. Introduction

Raùl Pateras Pescara patented the Free-Piston engine in 1928 originally as a Free-Piston spark ignited air compressor [1]. It has not had a successful commercial history and its past has not been very promising. Modern times and the invention of contemporary computers have reignited interest in the original concept among businesses and R&D facilities. Applications of FPLG technology are expected in the fields of distributed and off-grid power generation, marine propulsion, drones, electric mobility and microgrids. In this last field, FPLGs can support electric charging stations and can be a viable solution as the energy source in series for hybrids drivetrain and as a range extender for Electric Vehicles (EVs).

Fig. 1 shows the main components of a Free-Piston device: a Combustion Chamber (CC), a rebound device and a mechanical load. Free piston engines can be based on Spark Ignition (SI), Compression Ignition (CI), or Homogeneous Charge Compression Ignition (HCCI) combustion processes. The scavenging, that is the gas exchange process in the CC, can be performed through different layout: uniflow, loop and crossflow [2]. The rebound device is typically a Gas Spring (GS), as sketched in Fig. 1, but it can also be a mechanical spring. It serves as an energy buffer between the expansion and compression strokes due to the absence of the crankshaft mechanism.

The load of a FPLG is an electromechanical conversion system based on LEM and one or more power converters [3]. The LEM can have a variety of architectural designs, but it is typically a linear permanent magnet (PM) machine in a single-sided, multi-sided, or tubular arrangement. Besides electricity generation, the electric drive controls the piston movement and ensure ongoing oscillations even under unusual conditions occur [4].

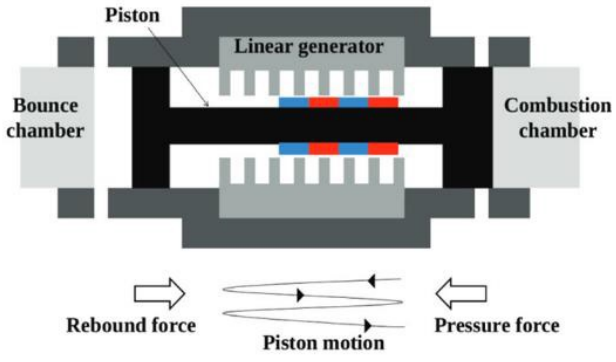

Fig. 1. FPLG structure.

This study was partly carried out within the Ecosistema MUSA - Multilayered Urban Sustainability Action and received partial funding from the European Union Next-GenerationEU (PIANO NAZIONALE DI RIPRESA E RESILIENZA (PNRR) – MISSIONE 4 COMPONENTE 2, INVESTIMENTO 1.5 – D.D. 1055 23/06/2022, ECS 00000037) and within the NEST - Network 4 Energy Sustainable Transition (D.D. 1243 02/08/2022, PE00000021) and received funding under the National Recovery and Resilience Plan (NRRP), Mission 4 Component 2 Investment 1.3, funded from the European Union - NextGenerationEU. This manuscript reflects only the authors' views and opinions, neither the European Union nor the European Commission can be considered responsible for them. All authors have contributed equally.

979-8-3503-4743-2/23/$31.00 ©2023 IEEE

Different architectures for this type of engine are possible, including single-piston, dual-piston, opposed-piston, W-shape, and many other ones [2]. The system dynamics should be optimized with at least three primary factors in mind:

- Moving Mass: in addition to technological limitations, the moving mass directly affects the piston's inertia and, thus, its motion.
- Compression Ratio: referred to as the ratio between the volumes within the CC (or GS) at the Top Dead Center (TDC) and the Bottom Dead Center (BDC). Thermal efficiency is typically proportional to compression ratio and it needs to be appropriately regulated for each type of burned fuel.
- Piston's stroke and Velocity: they significantly affect efficiency. In general, a larger stroke results in a higher speed and more room to accelerate, which increases power.

In addition to thermal energy control, a proper regulation of the electrical power by means of power converters is an essential way for controlling the dynamics of FPLG [5], [6]. Many control schemes focus on piston motion and electric power management at the same time, while other approaches divide these two aspects. The last configuration is preferred in applications, like onboard electrical vehicles, where a battery operates as a slack node balancing the power. In these cases, an active rectifier interfaces the LEM with the electric vehicle DC bus [7], [8].

This paper presents the integrated modelling of a FPLG. As the first step, the dynamic model of the FPLG has been developed in the opensource CFD software OpenFOAM and it is validated on the basis of the results presented in [3]. A gasoline single-piston SI Free-Piston ICE, a three-phase LEM and a resistive electrical load have been considered. Then, an active rectifier has been introduced into the electrical subsystem to obtain a stable DC voltage and its decoupled double-loop control founded on Space Vector Pulse Width Modulation (SVPWM) technique has been developed. The induced voltages, obtained as an output of the CFD model, have been included in the electric drive model that represents the LEM, the DC bus, the DC load and the active rectifier with its control; the latter has been implemented in Simulink.

II. Dynamic and thermodynamic model

A. Reference FPLG configuration

FPLG simulations were carried out on the engine developed by Toyota Central R&D Labs Inc. [2]–[4].As a result, the objective has been to develop and evaluate a model that can accurately imitate the dynamics of a free-piston engine and achieve the same level of performance. To do that, a gasoline SI single-piston W-shaped engine with a total power of 10 kW, as shown in Fig. 2, was developed in the OpenFOAM environment. Table I reports the main geometrical dimensions and main properties related to the reference free piston engine. According to these data, the piston-to-head clearance is defined to be 11 mm, with a cylinder maximum height of 111 mm, while the gas spring clearance results to be 33.33 mm. It is important to underline that the whole set of parameters and values is not available in the literature; missing parameters and missing values have been guessed and adjusted through sensitivity analysis to obtain results similar to the reference ones [2], [3].

TABLE I
Engine specification.

Engine bore	68 mm
Maximum stroke	100 mm
Internal stator diameter	120 mm
Scavenging ports height	25 mm
Total mass	4.8 kg

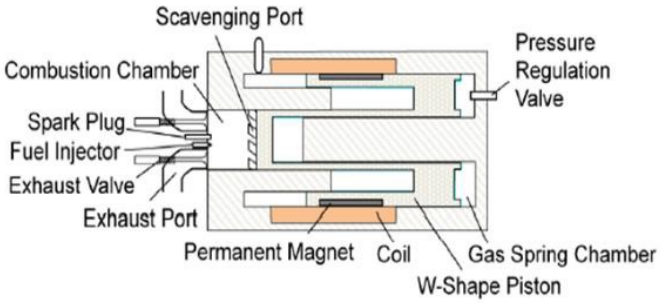

Fig. 2. Engine model configuration: single-piston W-shaped SI two-strokes engine [2].

B. CFD modelling

Despite OpenFOAM is a computer tool specific for CFD, it was used to simulate the interactions among the subsystem of the FPLG. As a matter of fact, is it possible to include in the OpenFOAM environment the equations representing both the dynamics and the equivalent electrical circuit of the FPLG; the latter requires the definition of a proper electrical load.

Figure 3 shows the models of both the combustion chamber and the gas spring: the former has been modelled as a cylinder slice with an angle of 2.5° whereas the latter has been modeled as an annulus shape thanks to the choice of a W-shaped piston.

C. Dynamic model

According to the Newton's second law, the piston motion results from the following forces applied to the FPLG:

$$m \cdot \left(\frac{d^2x}{dt^2} \right) = -F_{comb} + F_{gs} + F_{LEM} + F_{fric} \qquad (1)$$

where m is the total mass of the moving parts, x is the piston position, F_{comb} is the force acting on the piston due to the combustion process, F_{gs} is the force generated by the gas spring, F_{LEM} is the electromechanical force generated by the interaction between electric currents and magnetic field inside the LEM and F_{fric} is the friction force. The BDC is taken as the reference for the piston position, that increases towards the TDC. F_{comb} always pushes the piston towards the BDC, F_{gs}

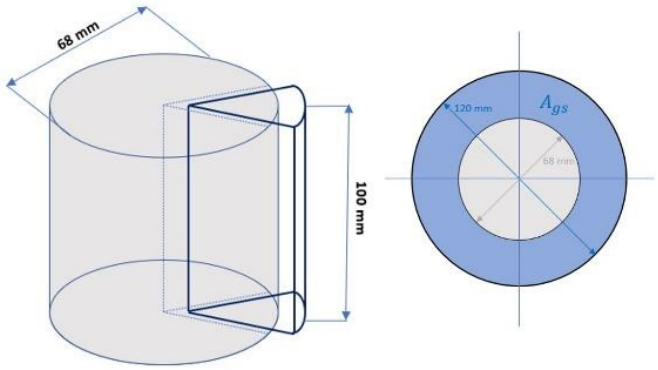

Fig. 3. Schematization of the modelled combustion chamber (left) and gas spring (right).

always pushes the piston towards the TDC, F_{fric} is always opposite to the velocity. The direction of F_{LEM} depends on the instantaneous values of the currents.

F_{comb} mostly depends on combustion heat release rate, that is represented by the Wiebe's function:

$$\frac{dQ}{dt} = H_u \cdot g_f \cdot \eta_c \cdot \frac{d\chi_B}{dt} \tag{2}$$

where H_u is the calorific value of fuel (octane in this work), g_f is the injected fuel mass per cycle, η_c is the combustion efficiency and $\frac{d\chi_B}{dt}$ is the derivative of the mass fraction burned during the combustion process [6]. The pressure and the temperature into the combustion chamber result as the solution of the CFD model, the volume of the combustion chamber changes over time according to the piston position.

The gas spring force F_{gs} can be estimated assuming adiabatic compression:

$$P_{gs} \cdot V_{gs}^{\gamma} = \text{const} \tag{3}$$

$$F_{gs} = A_{gs} \cdot P_{gs} \tag{4}$$

where γ is the ideal gas heat capacity ratio, A_{gs} is the gas spring cross section area, V_{gs} is the gas sping volume that changes over time according to the piston position and P_{gs} is the resulting pressure.

The equivalent circuit of a phase of the LEM is the series connection of a voltage source representing the induced voltage due to the piston motion, ε_{ind} , a resistor R_s representing the coil resistance and an inductor L_s representing the leakage inductance. The voltage induced on a coil is:

$$\varepsilon_{ind} = H \cdot N_t \cdot M_p \cdot \frac{\mu_0}{g_e} \frac{8}{\pi^2} \sin\left(\frac{\pi\tau}{2\tau_p}\right) \cdot \sin\left(\frac{\pi}{\tau_p}x\right) \frac{dx}{dt} \tag{5}$$

where H is the coil length, N_t is the number of turns per coil, M_p is the maximum value of the Magneto Motive Force (MMF) in the air gap, μ_0 is the vacuum magnetic permeability, g_e is the length of the air gap, τ_p is the pole pitch and τ is the permanent magnets width.

TABLE II
LEM MAIN PARAMETERS.

Parameter	Value
τ	50 mm
τ_p	30 mm
H_c	960 A/mm
g_e	33 mm
N_t	118
H	300 mm
R_S	0.16 Ω
L_S	0.67 mH

TABLE III
MAIN OUTPUTS FOR PROPOSED MODEL VALIDATION.

	Toyota [2], [3]	**Proposed model**	$\Delta\%$
Frequency (Hz)	26	28.32	+8.92%
Power (W)	10000	9996	-0.04%
Thermal Eff. (%)	42	46	+9.52%
CR cc	10	10.19	+1.9%
CR gs	4	4.01	+0.25%

The dynamic model of the electric circuit, in case of balanced three phase operation and in case of a load consisting of a three-phase resistor bank, is:

$$\varepsilon_{ind,k}(t) = i_{L,k}(t) \cdot (R_s + R_{load}) + L_s \cdot \frac{di}{dt} \tag{6}$$

the subscript k refers to the phase, R_{load} is the load resistance, and $i_{L,k}(t)$ is the LEM line current in phase k. The overall electromechanical force is:

$$F_{LEM} = 2 \cdot H \cdot N_t \cdot B_m \cdot \left(i_a(t) \cdot \sin\left(\frac{\pi}{\tau_p}x\right) + i_b(t) \cdot \sin\left(\frac{\pi}{\tau_p}x - \frac{2\pi}{3}\right) + i_c(t) \cdot \sin\left(\frac{\pi}{\tau_p}x + \frac{2\pi}{3}\right)\right) \tag{7}$$

where B_m is the maximum flux density in the air gap. Table II reports the data of the LEM.

F_{fric} can be expressed as: (8)

$$F_{fric} = -C_f \cdot \frac{dx}{dt} \cdot sgn\left(\frac{dx}{dt}\right) \tag{8}$$

where C_f is the friction coefficient, in this work set to 12 $\left[\frac{N \cdot s}{m}\right]$. The minus sign and the sign function allows to represent a force whose direction is always opposite to the piston velocity $\frac{dx}{dt}$.

D. Model results

Table III shows the main simulation results and compare them with the target results from Toyota prototype [2], [3]. A good agreement has been achieved, the small differences are correlated both to the estimated values of the missing parameters and to the different modelling approach.

Fig. 4 shows the steady state operation of the FPLG in terms of piston position, piston velocity, electromagnetic force and the set of three-phase (line to neutral) induced voltages. The piston

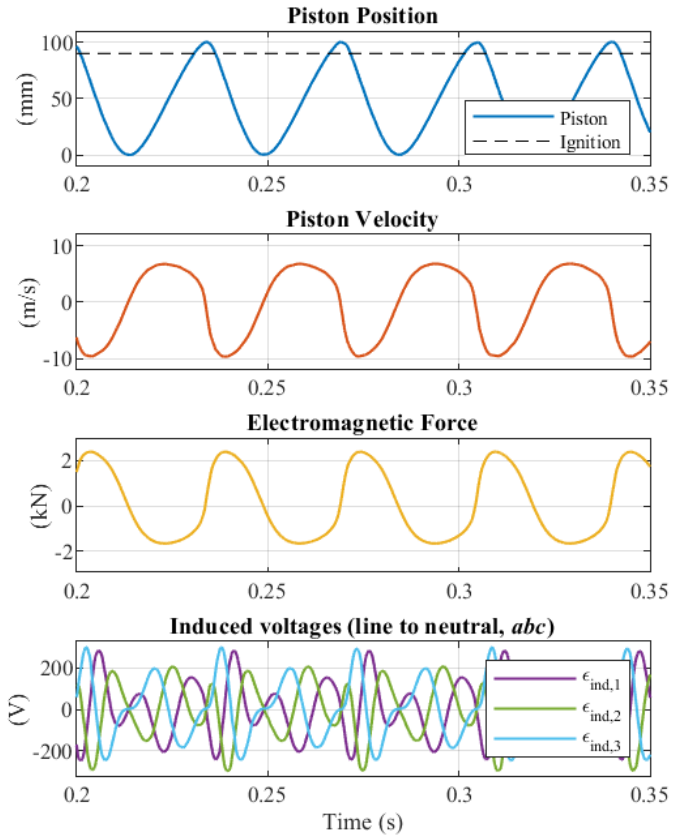

Fig. 4. Main results of the CFD model: piston position and velocity, electromagnetic force and set of line-to-neutral induced voltages.

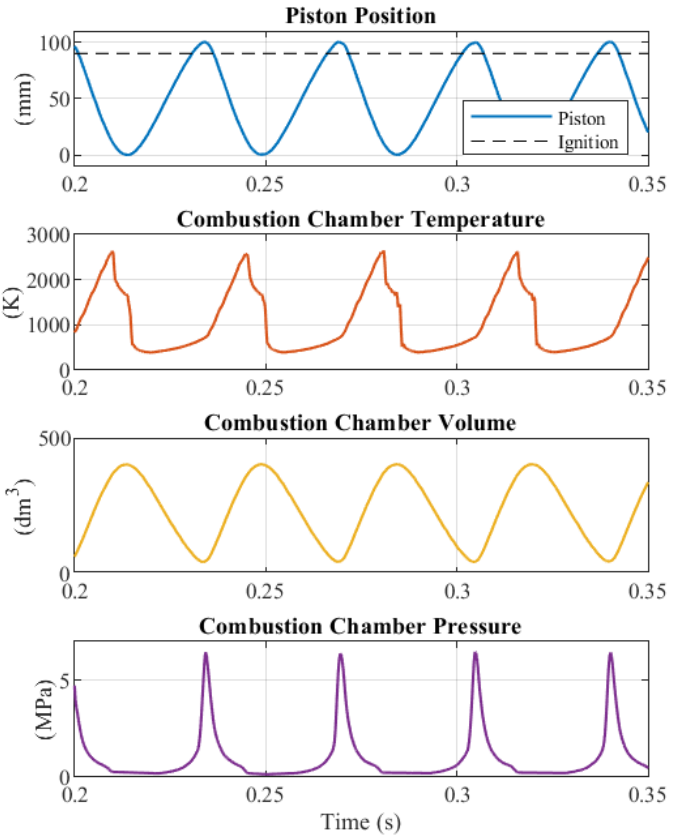

Fig. 5. Main results of the CFD model: piston position, thermal chamber temperature, volume and pressure.

position varies according to a non-sinusodal function, unlike a traditional ICE. Piston velocity and the electromechanical force have the same shape, but of opposite sign. Actually, the electromagnetic force acts in a similar way to a viscous force. This result is specific to the electrical subsystem considered in this work, in particular to the electrical load. Since the contribution of the leakage inductance is negligible, the line currents are actually proportional to the induced voltages, which in turn are proportional to the piston velocity. Being the electromagnetic force proportional to the current, it follows that the force is proportional to the piston velocity. The voltage waveforms highlights the differences in the piston motion between compression and expansion stroke. The expansion stroke is faster than the compression stroke, resulting in higher peaks of the induced voltages. Furthermore, the reversal of motion corresponds to the reversal of the sequence of the three-phase system.

Fig. 5 shows the temperature, the volume and the pressure of the combustion chamber; piston position has been included for reference. The temperature do not exceed the typical maximum values of the ICE technologies, being the maximum temperature achieved slightly above $2500\ K$. Moreover, it is worth mentioning that the faster expansion stroke and the resulting smaller resident time around TDC than a conventional engine based on crank-rod mechanism lead to a reduction in thermal losses and pollutant emissions [9]. Likewise, the maximum in-cylinder pressure is around $65\ bar$, which is similar to the technical limits of conventional ICE technologies. The small pressure drop right before the BDC represents the exhaust ports opening and the beginning of scavenging process.

III. Electric Power Conversion

Automotive sector is one of the most promising application fields for FPLG, as it can be a viable solution as power unit or as range extender in hybrid electric vehicles. In these electric vehicle layouts, usually a $400V$ or $800V$ DC bus interfaces the power source with the battery, propulsion system or other DC loads. The most suitable power converter to interface the LEM with the vehicle DC bus is the three-phase active rectifier. A suitable control logic has to be considered, such as constant DC voltage, constant DC power and so on, to regulate the power flow between LEM and DC bus. In this work, active rectifier is controlled to keep the DC bus voltage constant.

A. Kirchhoff's laws

Fig. 6 shows the electrical circuit modelling the LEM, the active rectifier and the DC load. The Kirchhoff's Voltage (KVL)

and current laws (KCL) are:

$$L_s \cdot \frac{di_a}{dt} = u_a - R_s \cdot i_a - \frac{u_{DC}}{3}(2S_a - S_b - S_c) \quad (9)$$

$$L_s \cdot \frac{di_b}{dt} = u_b - R_s \cdot i_b - \frac{u_{DC}}{3}(2S_b - S_a - S_c) \quad (10)$$

$$L_s \cdot \frac{di_c}{dt} = u_c - R_s \cdot i_c - \frac{u_{DC}}{3}(2S_c - S_a - S_b) \quad (11)$$

$$C \cdot \frac{du_{DC}}{dt} = S_a i_a + S_b i_b + S_c i_c - \frac{u_{DC}}{R_{load}} \quad (12)$$

where u_{DC} is the DC-side voltage, C is the DC-link capacitor, i_k are the line currents ($k = a, b, c$), u_k are the line-to-neutral induced voltages and S_k represent the switching states of the inverter ($S_k = 1$ corresponds to the upper switch in ON state, while $S_k = 0$ corresponds to the lower switch in ON state, k identifies the inverter leg). In this work, the induced voltages calculate by the OpenFOAM model are taken into account.

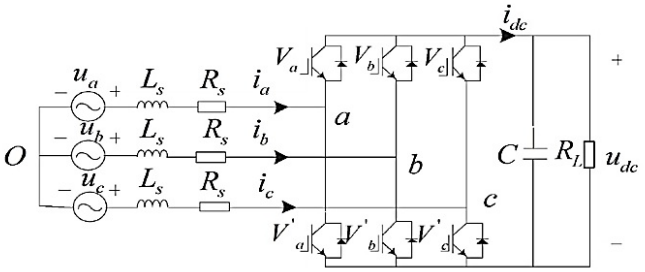

Fig. 6. Electrical circuit modelling the LEM, the active rectifier and the DC load.

The Park Transform converts the time-domain components of the three-phase system (eq. 9, 10 and 11) to the direct-quadrature-zero $dq0$ frame. The zero-sequence current is zero for topological reasons, thus the direct- and quadrature-sequence components are enough to fully represent the three-phase system. The dynamic model of the electrical subsystem in the $dq0$ frame is:

$$u_d = R_s \cdot i_d + L_s \cdot \frac{di_d}{dt} - \omega \cdot L_s \cdot i_q + v_d \quad (13)$$

$$u_q = R_s \cdot i_q + L_s \cdot \frac{di_q}{dt} - \omega \cdot L_s \cdot i_d + v_q \quad (14)$$

$$C \cdot \frac{du_{DC}}{dt} = \frac{3}{2}(i_d \cdot S_d + i_q \cdot S_q) - \frac{u_{DC}}{R_{load}} \quad (15)$$

where ω is the angular speed of the dq frame, v_d and v_q are the Park vector components of the inverter AC side voltage, S_d and S_q are the dq-axis switch function.

B. Double-loop active rectifier control scheme

Fig. 7 shows the double-loop active rectifier control scheme adopted to control the electric power conversion. The inner current loop and the outer voltage loop allow to define the set of three-phase voltages on the inverter AC side so that the DC load voltage is kept constant. The Park vector components, v_d and v_q, of the inverter AC side voltage are:

$$v_d = u_d - \left(K_p + \frac{K_i}{s}\right)(i_d^* - i_d) + \omega \cdot L_s \cdot i_q \quad (16)$$

$$v_q = u_q - \left(K_p + \frac{K_i}{s}\right)(i_q^* - i_q) + \omega \cdot L_s \cdot i_d \quad (17)$$

$$i_d^* = \left(K_{pv} + \frac{K_{iv}}{s}\right) \cdot (u_{DC}^* - u_{DC}) \quad (18)$$

where K_p and K_i are the PI current controllers gains, K_{pv} and K_{iv} are the PI voltage controller gains, and $i_d{}^*$ and $i_q{}^*$ are the Park vector components of the reference currents. In this work, u_{DC}^* has been set to $800V$ and i_q^* is zero to obtain unity power factor.

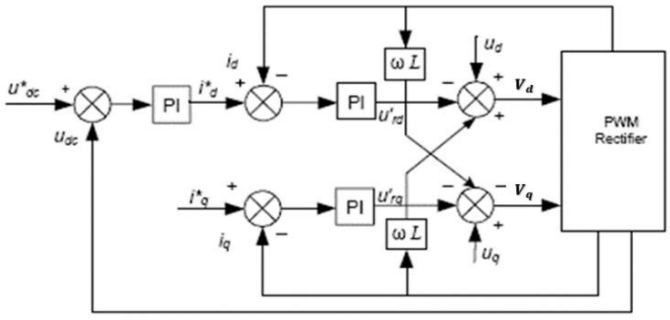

Fig. 7. Block diagram of the double-loop active rectifier control.

The Park vector obtained from eq. 16 and 17 has been referred to the $\alpha\beta$ coordinate space and the Clarke vector has been processed by the SVPWM generator that produce the proper switching sequence.

C. Model results

Fig. 8 shows the space vector in a stationary $\alpha\beta$ reference during a full cycle: it is zero both at the BDC and at the TDC, rotates clockwise during the compression stroke and rotates counterclockwise during the expansion stroke.

Fig. 9 shows the magnitude, the angular position and the angular speed of the space vector representing the induced voltages; piston position and the induced voltages in the abc frame have been reported as a reference. The space vector angular speed corresponds to the dq frame angular speed that allows to keep the Park vector aligned with the d-axis. Discontinuities in the angular position correspond to the change of the sequence.

Fig. 10 shows the regulated DC voltage, whose average is close to $800V$, and highlight the small voltage ripple; the latter result also depends on the $20000\mu F$ DC bus capacitance operating as an energy buffer.

Fig. 11 shows the phase a induced voltage and the line current. Current and voltage waveforms are in phase, and the higher the peak of the voltage waveform, the lower the peak of the current waveform. This is a result of the power flow regulation between LEM and DC load by the active rectifier.

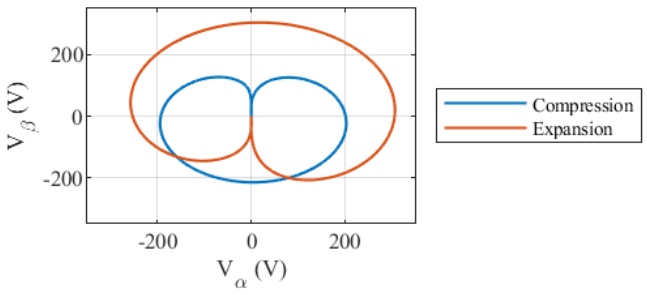

Fig. 8. Induced voltages space vector.

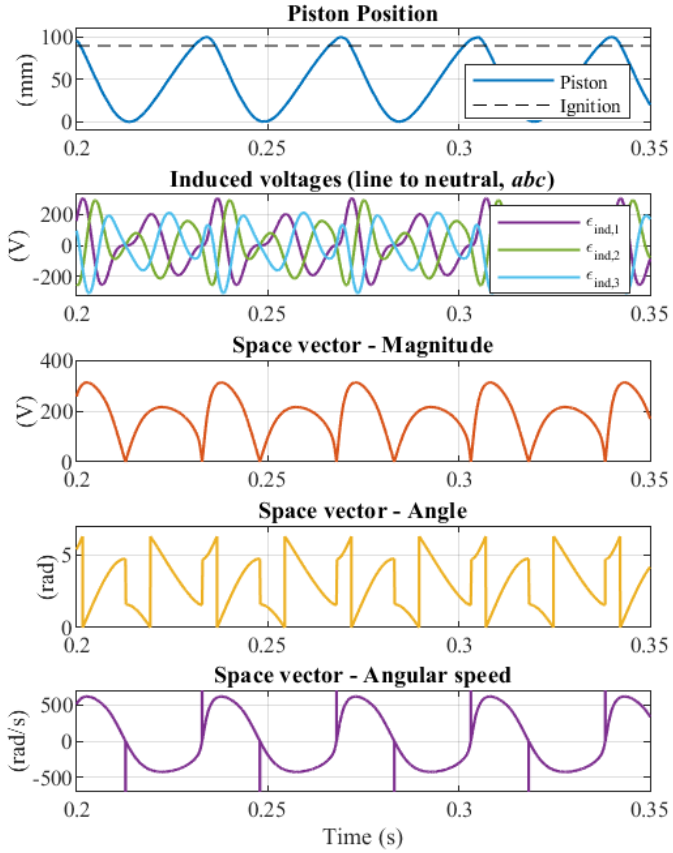

Fig. 9. Induced voltages space vector: magnitude, angular position and angular speed.

IV. Conclusions

The integrated dynamic modelling of a Free-Piston linear generator powering the DC bus of an electric vehicle has been presented. Although the proposed modelling methodology refers to the specific case study, it can be easily adapted to different FPLG configurations.

The CFD software allowed the accurate ICE modelling, representing the fluid-dynamic, the air-fuel mixture, the combustion process, the mechanical dynamics and a basic dynamic electric circuit in the same simulation tool. The modelling of the electric drive and its control required a proper simulation tool; in this work Matlab Simulink and SimPowerSystems library have been used.

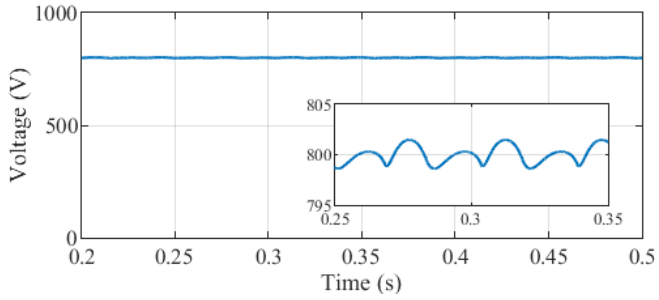

Fig. 10. DC bus voltage.

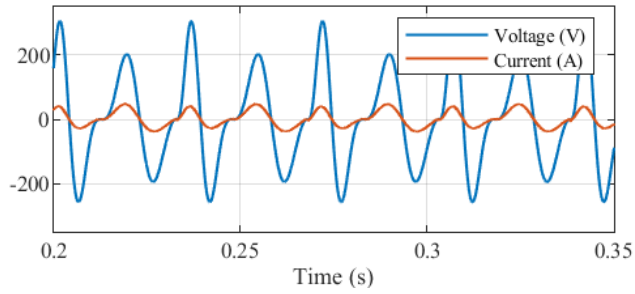

Fig. 11. AC-side induced voltage and line current.

The results show the effectiveness of an active rectifier to convert the non-sinusoidal AC voltages generated by the LEM into a stable DC voltage suitable for supplying the DC bus of an electric vehicle. This result is based on the hypothesis that the piston motion is little influenced by the type of electrical load, despite the electrodynamic force depends on the instantaneous value of the AC currents. Future works will investigate this assumption in more detail.

References

[1] R. P. Pescara, "Motor compressor apparatus," Patent U.S. 1,657,641, 1928.

[2] H. Kosaka, T. Akita, K. Moriya, S. Goto, Y. Hotta, T. Umeno, and K. Nakakita, "Development of free piston engine linear generator system part 1-investigation of fundamental characteristics," SAE Technical Paper, Tech. Rep., 2014.

[3] S. Goto, K. Moriya, H. Kosaka, T. Akita, Y. Hotta, T. Umeno, and K. Nakakita, "Development of free piston engine linear generator system part 2-investigation of control system for generator," SAE Technical Paper, Tech. Rep., 2014.

[4] K. Moriya, S. Goto, T. Akita, H. Kosaka, Y. Hotta, and K. Nakakita, "Development of free piston engine linear generator system part3-novel control method of linear generator for to improve efficiency and stability," SAE Technical Paper, Tech. Rep., 2016.

[5] P. Sun, C. Zhang, J. Chen, F. Zhao, Y. Liao, G. Yang, and C. Chen, "Hybrid system modeling and full cycle operation analysis of a two-stroke free-piston linear generator," *Energies*, vol. 10, no. 2, p. 213, 2017.

[6] C. Zhang, F. Chen, L. Li, Z. Xu, L. Liu, G. Yang, H. Lian, and Y. Tian, "A free-piston linear generator control strategy for improving output power," *Energies*, vol. 11, no. 1, p. 135, 2018.

[7] Y. Lu, X. Huang, and Z. Zhu, "Direct power control of a permanent magnet linear generator in a free piston energy converter," 2008, Conference paper, p. 3636 – 3639.

[8] L. Mao, C. Zhang, Y. Gao, P. Sun, J. Chen, and F. Zhao, "Dc bus voltage control of a free-piston linear generator," 2016.

[9] C. Yuan, H. Feng, Y. He, and J. Xu, "Combustion characteristics analysis of a free-piston engine generator coupling with dynamic and scavenging," *Energy*, vol. 102, p. 637 – 649, 2016.